Biomaterials Translational

Enhanced angiogenesis in porous poly(ε-caprolactone) scaffolds fortified with methacrylated hyaluronic acid hydrogel after subcutaneous transplantation

Huaxin Yang[1], Mengjia Zheng[1], Yuyue Zhang[1], Chaochang Li[2], Joseph Ho Chi Lai[1], Qizheng Zhang[1], Kannie WY Chan[1], Hao Wang[2], Xin Zhao[3], Zijiang Yang[2,], Chenjie Xu[1,*]*

Key Words:
angiogenesis; cell transplantation; hyaluronic acid; poly(ε-caprolactone); scaffold

From the Contents

ABSTRACT

A composite scaffold composed of a porous scaffold and hydrogel filling can facilitate engraftment, survival, and retention in cell transplantation processes. This study presents a composite scaffold made of poly(ε-caprolactone) (PCL) and methacrylated hyaluronic acid (MeHA) hydrogel and describes the corresponding physical properties (surface area, porosity, and mechanical strength) and host response (angiogenesis and fibrosis) after subcutaneous transplantation. Specifically, we synthesise MeHA with different degrees of substitution and fabricate a PCL scaffold with different porosities. Subsequently, we construct a series of PCL/MeHA composite scaffolds by combining these hydrogels and scaffolds. In experiments with mice, the scaffold composed of 3% PCL and 10–100 kDa, degree of substitution 70% MeHA results in the least fibrosis and a higher degree of angiogenesis. This study highlights the potential of PCL/MeHA composite scaffolds for subcutaneous cell transplantation, given their desirable physical properties and host response.

***Corresponding authors:**
Chenjie Xu,
chenjie.xu@cityu.edu.hk;
Zijiang Yang,
zijiang.yang@live.com

http://doi.org/10.12336/biomatertransl.2024.01.006

How to cite this article:
Yang, H.; Zheng, M.; Zhang, Y.; Li, C.; Lai, J. H. C.; Zhang, Q.; WY Chan, K.; Wang, H.; Zhao, X.; Yang, Z.; Xu, C. Enhanced angiogenesis in porous poly(ε-caprolactone) scaffolds fortified with methacrylated hyaluronic acid hydrogel after subcutaneous transplantation. *Biomater Transl.* **2024**, *5*(1), 59-68.

Introduction

Cell therapy has significant potential to revolutionise medicine by offering novel treatments for various diseases, such as cancer and endocrine and neurological disorders.[1, 2] The delivery method plays a critical role in the success treatment by influencing cell viability, biodistribution, and retention. At present, common delivery routes include intravenous/intra-arterial infusion and direct intra-tissue injection. In this field, scaffold-based transplantation is emerging as an alternative strategy for enhancing engraftment, survival, and retention.[3]

An ideal scaffold for cell delivery should exhibit biocompatibility, biodegradability, and adherence to cells to serve as a suitable substrate for cell attachment, proliferation, differentiated function, and migration.[4] A promising approach to meet these requirements is to combine a porous scaffold backbone with hydrogel filling.[5] This composite design consists of a stiff and porous backbone that provides mechanical stiffness and a two-dimensional environment. The scaffold backbone is then perfused with a soft hydrogel to provide a three-dimensional environment with chemistry that facilitates cell attachment, growth, and differentiation.

Poly(ε-caprolactone) (PCL) is a widely investigated polymer for scaffold fabrication owing to its favourable biocompatibility, ease of processing, and non-toxic degradation products.[6] Porous PCL scaffolds can be prepared through various techniques, such as three-dimensional printing, particulate leaching, phase separation, and electrospinning, to control the pore size

and porosity. Hyaluronic acid (HA)-based hydrogel is another commonly used biomaterial because of its biofunctionality, multiple reactive functional groups, and degradability. Research has demonstrated that HA hydrogel can promote angiogenesis and tissue regeneration.[7] Several researchers have combined porous PCL scaffolds with HA hydrogel to construct composites for cell transplantation.[8] However, this line of research is still in the nascent stage, and the influence of HA size on the *in vivo* performance of this composite remains to be clarified.

This study addresses this research gap by developing PCL/HA composite scaffolds and investigating their status after transplantation. Specifically, we synthesise methacrylated HA (MeHA) hydrogels with a range of crosslinking degrees and fabricate PCL scaffolds with different porosities. Subsequently, a series of PCL/MeHA composite scaffolds are prepared by combining the hydrogels and scaffolds. The fibrosis and vascularisation on these scaffolds after subcutaneous transplantation are explored to clarify the influence of the MeHA molecular weight, degree of substitution (DS), and pore size of the PCL scaffold on the scaffold performance (**Figure 1**). Quantification of the fibrous capsule thickness on the scaffold and von Willebrand factor (vWF) staining of the blood vessels in the fibrous capsule demonstrate that a composite scaffold composed of low molecular weight MeHA hydrogel and a PCL scaffold with smaller surface area and porosity exhibits the least fibrosis and enhanced angiogenesis.

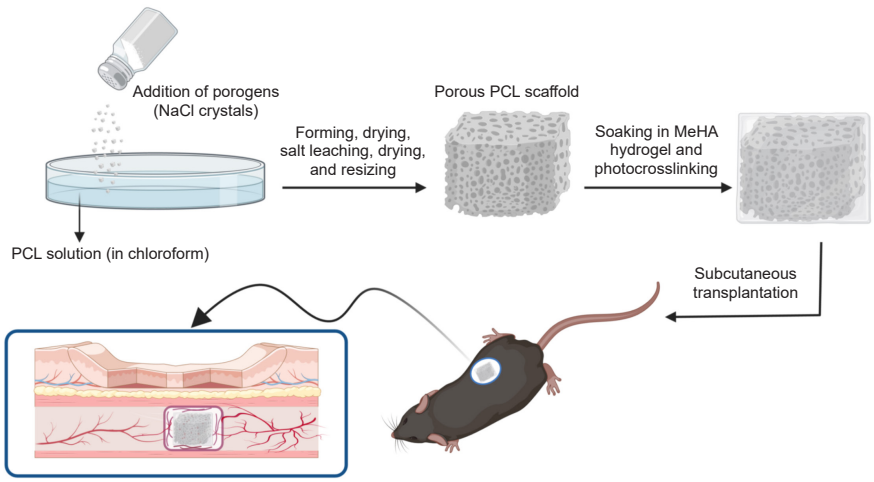

Figure 1. Fabrication and subcutaneous transplantation of PCL/MeHA composite scaffolds. Created with BioRender.com. MeHA: methacrylated hyaluronic acid; NaCl: sodium chloride; PCL: poly(ε-caprolactone).

Methods

Synthesis and characterisation of MeHA

Methacrylation of sodium HA (M_w 10–100, 200–400, and 900 kDa; Bloomage Biotechnology Co. Ltd., Beijing, China) was performed with reference to our previous work.[9] Specifically, 4.0 g HA was dissolved in 200 mL distilled water in a 500 mL three-necked round-bottom bottle and stirred overnight at 4°C. Subsequently, 133.3 mL N, N-dimethylformamide (Sigma-Aldrich, Burlington, MA, USA) was added in the HA solution, followed by the dropwise addition of 4.76 mL methacrylic anhydride (94%, Sigma-Aldrich). The pH of the solution was adjusted to 8–9 with fresh 1 M sodium hydroxide (NaOH, J&K Scientific Ltd., Beijing, China), and the mixture was stirred overnight at 4°C. Next, 9.88 g sodium chloride (NaCl; J&K Scientific) was added to attain a NaCl concentration of 0.5 M, and MeHA precipitated upon the addition of 1000 mL ethanol. The precipitated MeHA was washed three times with ethanol and then dissolved in 150 mL distilled water. In this manner, the unreacted methacrylic anhydride was removed by ethanol precipitation. The solution was dialysed against distilled water for 7 days, and the obtained purified product was lyophilised and characterised by ^{1}H spectroscopy (Bruker Avance II 400 MHz NMR, Billerica, MA, USA). The DS was determined using the signals of the methacryloyl group at 5.62 and 6.06 ppm (ascribed to anomeric protons of the double bond) and the methacrylate group at 1.83 ppm. The chemical shift of the methyl group connecting to the amide group was 1.90 ppm.

Preparation and rheological analysis of MeHA solution and hydrogels

MeHA solution, consisting of MeHA (50 mg/mL) and a photoinitiator (0.5 mg/mL, Irgacure 2959, Sigma-Aldrich), was dissolved in distilled water. MeHA hydrogels were prepared by exposing the MeHA solution to ultraviolet light (wavelength =

1 Department of Biomedical Engineering, City University of Hong Kong, Hong Kong Special Administrative Region, China; 2 Center for Pluripotent Stem Cell Research and Engineering, Research Institute of Tsinghua, Guangzhou, Guangdong Province, China; 3 Department of Applied Biology and Chemical Technology, The Hong Kong Polytechnic University, Hong Kong Special Administrative Region, China

360 nm, intensity = 10.0 mW/cm^2) for 10 minutes to achieve radical polymerisation.[10] The mechanical properties of the MeHA solution and hydrogels were determined by their storage modulus (G') and loss modulus (G''), measured using a rotating rheometer (Bohlin Instruments, Worcestershire, UK) in the frequency sweep mode of 0.1–10 Hz.

Swelling ratio of photocrosslinked MeHA

MeHA (50 mg/mL) and a photoinitiator (0.5 mg/mL, Irgacure 2959) were dissolved in distilled water. The mixture was cast into a plasma-treated polydimethylsiloxane (Dow Corning 184 Sylgard) mould (diameter: 15.82 mm, thickness: 1.04 mm) until the cavity was filled. Subsequently, the polydimethylsiloxane mould was centrifuged at 753 × g (with g representing the relative centrifugal force) for 2 minutes to ensure uniform distribution of the material (Sorvall ST 16R Centrifuge, Thermo Fisher Scientific Inc., Waltham, MA, USA). After drying at room temperature (approximately 25°C) in a fume hood (approximately 12 hours), dry MeHA plates were carefully separated from the polydimethylsiloxane mould, trimmed to a circle with a diameter of 12 mm, and exposed to ultraviolet light (wavelength = 360 nm, intensity = 10.0 mW/cm^2) for a certain period (3, 5, or 15 minutes).

The swelling properties of the MeHA plates were determined in phosphate-buffered saline (PBS) at 37°C.[11] The wet weight of the MeHA plates was measured at several time points during the incubation. The swelling ratio was calculated as $(W_s - W_i)/W_i \times 100$,[12] where W_s represents the weight of the swollen hydrogel at a given time point and W_i represents the weight of the dried hydrogel at 0 seconds.

Fabrication of PCL scaffolds

PCL scaffolds were fabricated through solvent casting and salt leaching.[13-16] A 5% (w/v) PCL solution was prepared in chloroform (J&K Scientific), and NaCl was added to the PCL solution at various ratios (PCL:NaCl = 7:93, 6:94, 5:95, 3:97, and 2:98). The required amount of NaCl particles were placed in sterile Petri dishes, and the solution was poured into each Petri dish while ensuring even distribution. The dishes were placed in the fume hood overnight to allow the solvent to evaporate. To remove the salt particles, polymer sheets (thickness = 2 mm) were extensively washed using a sonicator (DTC-10J, Toptill Technology, Hubei, China) with sterile distilled water. Finally, the dried polymer sheets were cast and resized into samples sized 10 mm × 5 mm. The scaffold porosity was evaluated using the theoretical approach proposed by Landers et al.[17] Porosity (%) = $(1 - V_{PCL}/V_{Scaffold}) \times 100$.

Mechanical testing of PCL scaffolds

The mechanical properties of the PCL scaffolds were measured using a computer-controlled Instron Tensile 5942 Micro Tester (Instron, Norwood, MA, USA). Compressive tests were conducted at room temperature with a 1 kN load cell at a crosshead speed of 1 mm/min, and tensile tests were performed at a crosshead speed of 3 mm/min. The elastic modulus (both tensile and compressive) was calculated from the initial slope of the stress–strain curve within the elastic deformation range. Preloading was performed before the test to prevent plastic deformation of the porous structure. Measurements were obtained for three samples of each type.[18]

Scanning electron microscopy examination of PCL scaffolds

All of the samples were coated with gold using a Q150TS dual-target sputtering system (Quorum, East Sussex, UK).[19] Scanning electron microscopy (SEM) images were obtained using an FEI Quanta 250 e-SEM microscope (Bruker, Billerica, MA, USA) with an electron landing voltage of 10 kV.

Nitrogen adsorption and desorption measurements for Brunauer–Emmett–Teller surface area analysis

The scaffolds were degassed prior to the measurement. Data were collected using V-Sorb 2800TP (Gold APP Instruments Co., Beijing, China) by the multi-point Brunauer–Emmett–Teller (BET) testing method. The surface area was calculated using the BET method. The total pore volume of single-point adsorption was calculated from adsorption isotherms using the following formula: Total pore volume = gas amount adsorbed at P/P_0 = 0.99 or 0.995 at specific gas densities. Where P is the equilibrium adsorption pressure of the gas, and P_0 denotes the saturated vapour pressure of the gas at the adsorption temperature.

In vitro biocompatibility test

To prepare PCL/MeHA composite scaffolds, MeHA (50 mg/mL) and a photoinitiator (Irgacure 2959, 0.5 mg/mL) were dissolved in low-glucose Dulbecco's modified Eagle's medium (Thermo Fisher Scientific Inc.) containing 1% penicillin–streptomycin and 10% foetal bovine serum (Invitrogen, Thermo Fisher Scientific Inc.). The pH was adjusted using 1 M NaOH. The PCL scaffold (sterilised through immersion in 75% ethanol solution for 30 minutes followed by exposure to ultraviolet irradiation for 30 minutes) was immersed into the MeHA solution to fill the pores. The MeHA hydrogel was then exposed to ultraviolet light (wavelength = 365 nm, intensity = 10.0 mW/cm^2) for 20 minutes (10 minutes for each side of the scaffold).

Mesenchymal stem cells (MSCs, Invitrogen) (1 × 10^5 cells per well) were cultured in a 24-well plate with PCL/MeHA scaffolds in a medium composed of 500 μL growth medium and 50 μL alamarBlue (cell viability reagent, Invitrogen). As a positive control, MSCs were cultured in the medium alone. After 18 hours of culture, 100 μL of the medium was extracted for cell viability analysis using a microplate reader (SpectraMax M5e multi-mode microplate reader, Molecular Devices, Silicon Valley, CA, USA).

Subcutaneous transplantation of PCL/MeHA scaffolds

Animal experiments were performed on C57bl/6 male mice (4–6 weeks old) in accordance with a protocol (Internal Ref: A-0654, approved on September 15, 2021) approved by the Animal Research Ethics Sub-Committee of City University of Hong Kong. Male mice were chosen owing to their higher biochemical uniformity and lower hormone fluctuations.

The PCL/MeHA composite scaffold was prepared similarly to those in the *in vitro* biocompatibility test, except the medium was changed to 1× PBS with 1% penicillin–streptomycin. Moreover, the blank PCL scaffolds were immersed in 1× PBS with 1% penicillin–streptomycin (10,000 U/mL, Corning Inc., Corning, NY, USA) before transplantation.

To obtain PCL/fibrin composite scaffolds,[13, 14] a 2 mg/mL mouse fibrinogen solution (Sigma-Aldrich) was prepared by dissolving mouse fibrinogen in CMRL medium (ThermoFisher) with 1% penicillin–streptomycin. The mouse fibrinogen solution (100 μL) was then mixed with 1 μL of 100 U/mL thrombin IIa (Sigma-Aldrich; in distilled water) and transferred to the PCL scaffold. The fibrin gel solidified within the scaffold after 1-hour incubation at room temperature followed by 1-hour incubation at 37°C.

The mice (C57bl/6, male, 4–6 weeks old, obtained from the Laboratory Animal Research Unit (LARU) of City University of Hong Kong) were anaesthetised with inhalational isoflurane (Piramal Critical Care Inc., Mumbai, MH, India). The induction and maintenance concentrations of isoflurane were 2.5–3 L/min and 1.5–2 L/min, respectively, with an oxygen flow rate of 1.5 L/min (Compact Small Animal Anesthesia Machine, RWD, Guangdong, China). Hair on the dorsum was removed, and the dorsum was sterilised with 70% ethanol (Watsons, Hong Kong Special Administrative Region, China) and Betadine (Mundipharma Pharmaceuticals Ltd., Cambridge, UK).[20] An initial longitudinal incision (1 cm in length) was created on the dorsal using a scalpel blade. A subcutaneous pocket was created through blunt dissection using forceps. Two scaffold discs were then inserted into the subcutaneous pocket, and the incision was closed with a suture line. All mice received post-surgery analgesia (ibuprofen (Sigma-Aldrich) once after transplantation, 5 mg/kg or 1 mg/mL provided by subcutaneous injection). After transplantation, the mice were reared in the LARU at City University of Hong Kong (temperature of 18–23°C with 40–60% humidity; 14-hour light/10-hour dark cycle).

Histology and immunohistofluorescence analysis

Four weeks after transplantation, scaffolds with surrounding tissues were removed and immersed in an optimal cutting temperature compound for embedding. The embedded blocks were cut into 5–10 μm thin sections using a microtome (CryoStar NX70 Cryostat, Thermo Fisher Scientific Inc.). These thin sections were subjected to haematoxylin & eosin (H&E) or immunostaining (vWF staining) according to the instructions provided with the staining kits. Specifically, in H&E staining, the samples were initially fixed with 10% paraformaldehyde (Sigma-Aldrich) for 10 minutes. Subsequently, the slides were stained with hematoxylin (Thermo Fisher Scientific Inc.) for 10 minutes and counterstained with eosin (Thermo Fisher Scientific Inc.) for 45 seconds. For vWF staining, acetone was used to fix the tissues and remove PCL (10 minutes at –20°C). The samples were then subjected to antigen retrieval in citrate buffer (Sigma-Aldrich) at 95°C for 10 minutes. Later, the samples were blocked with 10% normal goat serum (Sigma-Aldrich) and 1% bovine serum albumin (Thermo Fisher Scientific Inc.) in PBS-Tween 20 and then incubated overnight with the diluted anti-vWF antibody (1:100, Abcam, Cambridge, UK) in 1% bovine serum albumin PBS-Tween 20 in a humidified chamber at 4°C followed by 1-hour incubation in diluted secondary antibody (goat anti-rabbit anti-IgG, 1:500, Abcam) in 1% bovine serum albumin PBS-Tween 20 at room temperature in the dark. Finally, a fluorescence-mounting medium (containing 4′, 6-diamidino-2-phenylindole, Abcam) was dropped directly atop the specimen. Stained slides were imaged using a Nikon Eclipse Ti inverted microscope (Nikon, the Netherlands). The area of fibrous tissue was quantified using Fiji software (Version 2.14.0/1.54f for macOS, Fiji, National Institute of Mental Health, Bethesda, MD, USA).[21] The thickness of the fibrous tissue was calculated by dividing by dividing the area by the length. The number of blood vessels was also counted through the ImageJ software (National Institute of Mental Health).[22]

Statistical analysis

At least three sets of independent experiments were performed for each assay except the rheological analysis and animal experiments. One-way analysis of variance followed by Dunnett's multiple comparison test and simple linear regression were performed using GraphPad Prism (version 9.5.1 for macOS, GraphPad Software, San Diego, CA, USA, www.graphpad.com). *P* values less than 0.05 indicate significance.

Results

Synthesis and characterisation of MeHA

MeHA, a derivative of HA, was synthesised by conjugating methacrylic anhydride to the HA backbone. In 1H spectroscopy (**Additional Figure 1**), signals of the methacryloyl group were observed at 5.62 and 6.06 ppm (corresponding to the anomeric protons of the double bond). The DS was determined by the ratio of peak areas between the methyl group on the methacrylate group at 1.83 ppm and the methyl group connecting to the amide group at 1.90 ppm. Four types of MeHA with different DSs and molecular weights were synthesised: DS70% + 10–100 kDa MeHA (DS70-100 MeHA), DS37% + 200–400 kDa MeHA (DS37-400 MeHA), DS71% + 200–400 kDa MeHA (DS71-400 MeHA), and DS72% + 900 kDa MeHA (DS72-900 MeHA). These samples were divided into two groups: similar DS group (DS70-100, DS71-400, and DS72-900) and same molecular weight group (DS37-400 and DS71-400).

MeHA hydrogels were obtained by crosslinking the aqueous MeHA solution (50 mg/mL MeHA and 0.5 mg/mL photoinitiator) under ultraviolet irradiation (10.0 mW/cm^2) for 10 minutes to induce radical polymerisation. Viscoelastic properties of the derived MeHA hydrogels before and after crosslinking were studied through strain-controlled tests (**Figure 2A** and **B**). Additionally, viscoelastic properties of unmodified HA solutions with the same concentration were determined (**Additional Figure 2**). The loss modulus G'' and storage modulus G' of DS70-100, DS37-400, DS71-400, and DS72-900 MeHA solutions exhibited frequency-dependent behaviour, indicating their viscoelastic nature with both viscosity and elasticity.[23] Notably, the values of both moduli were small, reaching approximately 10 at a frequency of 10 Hz. Thus, these samples exhibited low viscosity and elasticity. G'' values of DS37-400 and DS71-400 MeHA were always smaller

than their G values, indicating their higher viscosity. However, no significant difference was observed between the G'' and G' values of the two solutions, indicating that the DS did not influence the viscoelastic properties of the MeHA hydrogels. In contrast, for the DS72-900 MeHA solution, the growth rate of G' was higher than that of G'' with increasing frequency. This trend indicated that the MeHA with higher molecular weight exhibited reduced mobility. Similar observations were derived from the rheological properties of unmodified HA solutions (**Additional Figure 2**), indicating the methacrylation did not change the rheological performance of HA in the solution state.

After crosslinking, G' of DS70-100 MeHA hydrogel remained in the range of 400–600 Pa, while G'' was approximately 100 Pa. The G'' and G' values of the other three hydrogels were 10 times higher than those of the DS70-100 MeHA hydrogel. These results confirmed the elastic solid nature of the hydrogels, with DS37-400, DS71-400, and DS72-900 MeHA hydrogels with larger molecular weights exhibiting a higher stiffness compared with the DS70-100 MeHA hydrogel.

Additionally, we investigated the swelling behaviour of MeHA wafers by comparing their mass before and after incubation in PBS. MeHA gels with an initial solid content of 5% (w/w), varying degrees of methacrylate substitution, and different molecular weights were prepared at room temperature, and their swelling was evaluated at room temperature. As shown in **Additional Figure 3**, regardless of the ultraviolet crosslinking time, the swelling of DS70-100, DS71-400, and DS72-900 MeHA hydrogels reached a plateau within 1 minute, whereas the DS37-400 MeHA showed saturation after 3 minutes. These findings indicate that the swelling rate was affected by the crosslinking degree, with a higher DS resulting in faster saturation. In the case of the same molecular weight group (DS37-400 and DS71-400 MeHA), DS71-400 MeHA with a higher DS exhibited a smaller swelling ratio. Next, the influence of ultraviolet exposure time on the swelling ratio was then investigated. Notably, DS71-400 MeHA with 3-minute ultraviolet exposure extracted liquid four times its own mass, whereas DS71-400 MeHA with 15-minute ultraviolet exposure only extracted liquid twice its original mass.

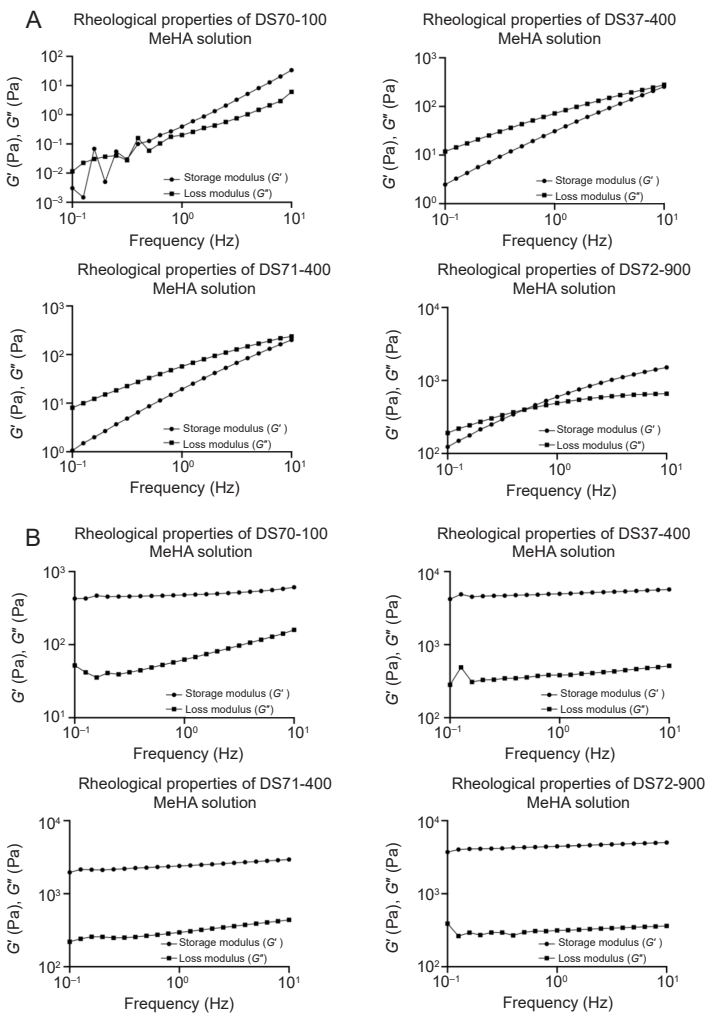

Figure 2. Characterisation of rheological properties. (A, B) Storage modulus (G') and loss modulus (G'') of MeHA solutions (5% (w/w); A) and derived MeHA hydrogels (B). Data corresponded to one experiment. DS: degree of substitution; MeHA: methacrylated hyaluronic acid.

Fabrication and characterisation of PCL scaffolds

PCL scaffolds were fabricated through solvent casting and salt leaching techniques.[13] Briefly, NaCl particles were homogeneously mixed with the PCL solution in a glass Petri dish. After the solution was dried, NaCl was removed by extensive washing. The scaffold was dried and then resized to 10 mm × 5 mm. The weight percentage of PCL in the PCL–NaCl mixture was tuned to 2%, 3%, 5%, 6%, and 7%. Thus, five PCL scaffolds using different proportions of PCL were fabricated and labelled as *x*% PCL scaffold, with x = 2–7.

SEM images of the PCL scaffolds revealed a porous structure (**Additional Figure 4**). However, the pores exhibited non-uniform sizes and shapes. We further examined the BET surface area and Barrett–Joyner–Halenda pore size distribution of these PCL scaffolds through nitrogen gas absorption. Adsorption and desorption isotherms were obtained (**Figure 3A**), and BET and Barrett–Joyner–Halenda analyses were performed (**Figure 3B**).

The porous PCL scaffolds exhibited a type III isotherm (**Figure 3A**) with no obvious saturated adsorption platform, suggestive of an irregular inner pore structure. This phenomenon typically occurs when a multimolecular layer forms on a hydrophobic surface or when the adsorption interaction between the solid and adsorbent is weaker than the interaction between the adsorbent molecules. At the same relative pressure, the 7% PCL scaffold absorbed/desorbed the highest quantity of nitrogen, while the 2% PCL scaffold absorbed/desorbed the least. The quantity of nitrogen absorbed/desorbed was positively correlated with the surface area and porosity: higher nitrogen absorption corresponded to a larger surface area and porosity of the scaffold. As the PCL concentration in the scaffold decreased from 7% to 2%, the quantity of nitrogen decreased, revealing that the 7% PCL scaffold exhibited the largest surface area and highest porosity.

As shown in **Figure 3B**, as the weight percentage of PCL in the mixture decreased, the scaffolds exhibited reduced surface area and porosity. However, the softness increased and mechanical support diminished when the PCL weight percentage was reduced from 7% to 2%, resulting in lower porosity of scaffold values. Therefore, even when more NaCl crystals were used to fabricate the scaffold, the porosity and surface area were decreased.

The mechanical properties of PCL scaffolds were investigated by tensile and compression tests (**Additional Figures 5** and **6**), and tensile and compressive moduli were calculated (**Figure 3C** and **D**). The tensile modulus of the 7% PCL scaffolds was 1.04 kPa, approximately 13 times that of the 2% PCL scaffolds (0.08 kPa) (**Figure 3C**). Scaffolds with lower PCL ratios (2% and 3%) had lower compressive moduli, although the difference was not significant (**Figure 3D**). The values of the compressive moduli ranged from 14.70 kPa to 32.37 kPa. The non-significant difference potentially resulted from the inner properties of the scaffolds and differences in tensile and compressive tests. The tensile properties at the vertical section were notably influenced by the ratio of PCL and NaCl, whereas the compressive modulus at the horizontal plane remained nearly unchanged.

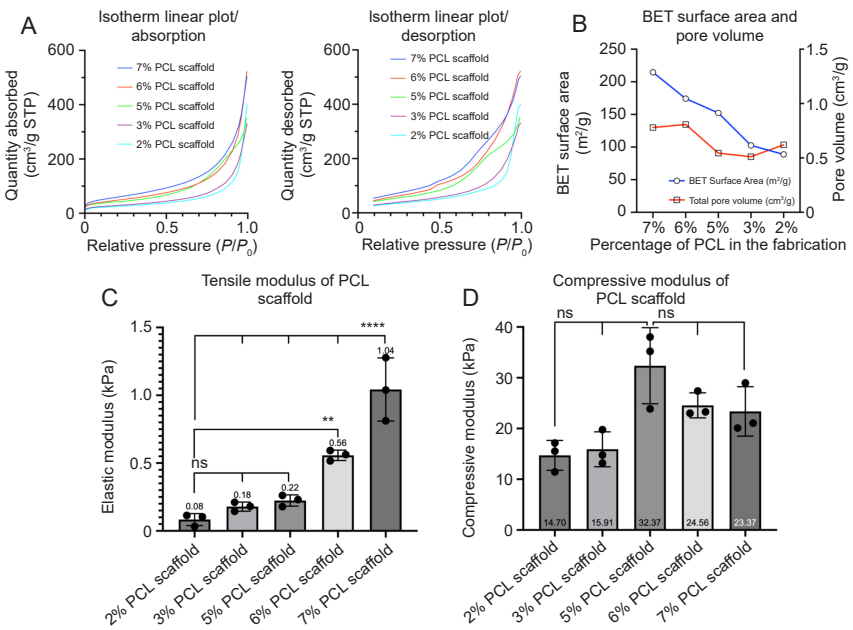

Figure 3. Characterisation of PCL scaffolds. (A) Isotherm linear plot of absorption and desorption of PCL scaffolds with different ratios of PCL and NaCl (number of samples per scaffold, n = 5). (B) BET surface area and pore volume of PCL scaffolds with different ratios of PCL and NaCl (n = 5). (C) Tensile moduli of PCL scaffolds with different ratios of PCL and NaCl (n = 3; three measurements were obtained per scaffold). (D) Compressive moduli of PCL scaffolds with different ratios of PCL and NaCl (n = 3; three measurements were obtained per scaffold). Data are expressed as mean ± SD. $^{**}P < 0.01$, $^{****}P < 0.0001$ (one-way analysis of variance followed by Dunnett's multiple comparison test). BET: Brunauer–Emmett–Teller; NaCl: sodium chloride; ns: not significant; P: the equilibrium adsorption pressure of the gas; P_0: the saturated vapour pressure of the gas at the adsorption temperature; PCL: poly(ε-caprolactone).

In vitro biocompatibility test of PCL/MeHA composite scaffolds

To test the applicability of the PCL/MeHA composite scaffolds, we investigated the viability of MSCs cultured with these scaffolds. The MSCs cultured with the PCL/MeHA composite scaffold showed higher viability than cells cultured alone (**Additional Figure** 7). Specifically, the cell viability values were 126.29%, 137.33%, 135.56%, and 140.11% for PCL/DS70-100, PCL/DS37-400, PCL/DS71-400, and PCL/DS72-900 MeHA scaffolds, respectively, indicating that these PCL/MeHA composite scaffolds were not cytotoxic.

Subcutaneous transplantation of PCL/MeHA composite scaffolds

The PCL/MeHA composite scaffolds were prepared by soaking porous PCL scaffolds in the MeHA solution followed by photocrosslinking. We selected the PCL scaffold containing 3% PCL for this experiment because of their softness and low tensile and compressive moduli, matching the mechanical properties of the host tissue.[4] However, all four MeHA hydrogels were used in the experiment.

The experiment involved seven groups, including a blank PCL scaffold group as the sham control, negative control, PCL/fibrin composite scaffold for positive control, and PCL/MeHA composite scaffolds (**Additional Figure 8A**). The blank PCL scaffolds were soaked in PBS (1×). The PCL/MeHA composite scaffolds were prepared by immersing PCL scaffolds into the MeHA solution (5% (w/w)) to fill the pores. The PCL/fibrin composite scaffold was prepared by immersing the PCL scaffold into a mixture of fibrinogen and thrombin IIa. The PCL/MeHA composite scaffolds were exposed to ultraviolet light to solidify MeHA, whereas the fibrin gel in the PCL/fibrin composite scaffold was formed through 1-hour incubation at room temperature followed by another 1-hour incubation at 37°C.

The PCL/MeHA composite scaffolds, blank PCL scaffold, and PCL/fibrin composite scaffold were implanted into subcutaneous pockets on the backs of 4–6-week-old male C57bl/6 mice in a randomised manner to minimise individual and location-based variations (two pieces of scaffolds per mouse, **Additional Figure 8B**). Four weeks after transplantation, the scaffolds were removed from the host mice for histological examinations (**Additional Figure 9**). Images revealed the formation of new blood vessels and fibrotic capsules of different thicknesses around the scaffolds. Notably, the fibrotic capsule around the PCL/DS72-900 MeHA composite scaffolds appeared slightly thicker compared with the others. H&E staining (**Figure 4A** and **B**) was performed to assess the general tissue structure and level of foreign body response (FBR).[24] Additionally, vWF staining (**Figure 5**) was performed to reveal the formation of capillary vessels (i.e., angiogenesis).

Four weeks after transplantation, collagen was deposited around the scaffolds, known as fibrosis.[25] The level of FBR was determined by measuring the thickness of the fibrosis capsule in the H&E stained images (**Figure 3A** and **B**). The scaffolds filled with MeHA hydrogels with lower molecular weights (100 and 400 kDa MeHA) induced mild fibrosis, with the average fibrous capsule thickness (< 190 μm) being similar to that of the blank PCL scaffold and PCL/fibrin composite scaffolds. However, the average fibrosis thickness of the device with 900 kDa MeHA was 517 μm owing to its high elasticity, high stiffness, and low swelling behaviour (**Additional Figure 2**), resulting in more severe FBR. The 900 kDa MeHA exhibited the highest G' and G'' values (**Figure 2**), indicating the highest stiffness. The sham group resulted in only mild fibrosis, with the fibrous capsule thickness being 57 μm.

Results of vWF staining (**Figure 5A**) indicated that all of the PCL/MeHA composite scaffolds (regardless of molecular weight and DS) successfully induced angiogenesis similar to the PCL/fibrin scaffolds. The PCL scaffold effectively induced the vascular regeneration. However, the ability of the blank PCL scaffold in inducing angiogenesis was slightly weaker than that of the PCL/MeHA composite scaffolds (**Figure 5B**). Notably, the PCL/DS70-100 MeHA scaffold induced larger and more apparent blood vessels compared with the PCL/DS72-900 MeHA scaffold. In summary, the PCL/DS70-100 MeHA scaffold, resulting in mild fibrosis and strong angiogenesis, represented the optimal configuration.

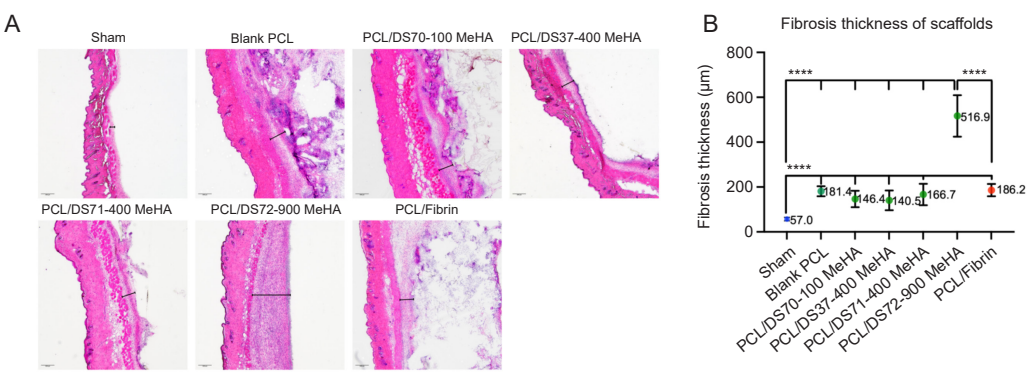

Figure 4. Histological evaluation of scaffold sections after four-week implantation in mice. (A) H&E staining results: interaction of scaffolds with surrounding tissues (microscopy images at 4× magnification; the black line segment indicates the fibrotic capsule). (B) Fibrosis thickness of different scaffolds based on images obtained at 4× magnification (samples per implant, $n = 3$, with five measurements obtained per implant). Data are expressed as mean ± SD. *$P < 0.05$, ****$P < 0.0001$ (one-way analysis of variance followed by Dunnett's multiple comparison test). DS: degree of substitution; H&E: haematoxylin & eosin; MeHA: methacrylated hyaluronic acid; ns: not significant; PCL: poly(ε-caprolactone).

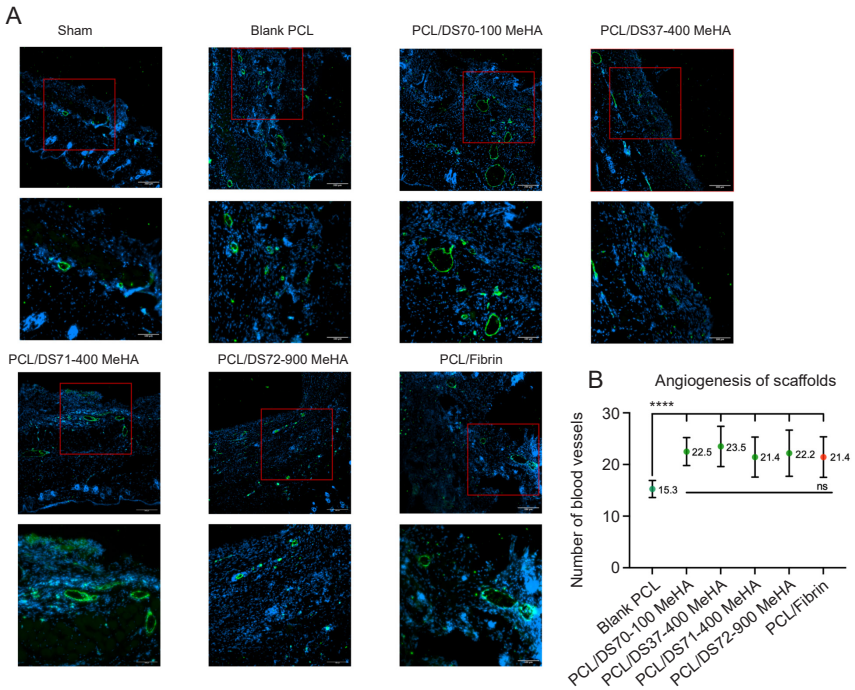

Figure 5. vWF staining results. (A) New blood vessels (microscopy images obtained at magnification of 10× (upper) and 20× (lower)). The square indicates the area chosen for amplification. All of the PCL/MeHA composite scaffolds (regardless of molecular weight and DS) successfully induced angiogenesis similar to the PCL/fibrin scaffolds. The PCL scaffold effectively induced the vascular regeneration. (B) Quantitative analysis of angiogenesis: number of blood vessels associated with different scaffolds based on 10× magnified images (samples per implant, $n = 3$, with five measurements obtained per implant). Data are expressed as mean ± SD. ****$P < 0.0001$ (one-way analysis of variance followed by Dunnett's multiple comparison test). DS: degree of substitution; MeHA: methacrylated hyaluronic acid; ns: not significant; PCL: poly(ε-caprolactone); vWF: von Willebrand factor.

Discussion

We fabricated a series of PCL/MeHA composite scaffolds composed of PCL (with different surface areas and porosities) and MeHA (with different sizes and DS). The corresponding physical properties (surface area, porosity, and mechanical strength) and host responses (angiogenesis and fibrosis) after subcutaneous transplantation were examined.

MeHA was selected as the base material because the crosslinking degree of MeHA can be readily tuned through the ultraviolet exposure time, facilitating the enhancement of angiogenesis. Methacrylation and subsequent crosslinking converted HA into a highly swellable gelator. Hydrogels derived from higher molecular weight MeHA exhibited higher stiffness and less swelling (**Figure 2** and **Additional Figure 3**). The porosity and mechanical strength of the PCL scaffold were modulated by changing the ratio of PCL and NaCl crystals in the solvent casting and salt leaching processes (**Figure 3B**). In general, PCL is a semi-crystalline polymer with a high degree of crystallinity.[26] At higher PCL ratios, the scaffold became more compact, leading to increased tensile modulus.[18, 27] Notably, unlike the tensile modulus, the compressive modulus did not change significantly as the PCL ratio varied (**Figure 3D**). This phenomenon may be attributable to the different responses of porous structures to compression and stretching. Additional studies must be performed to verify this hypothesis.

The assembled PCL/MeHA composite scaffolds, transplanted into subcutaneous pockets on the backs of mice, successfully induced mild fibrosis and angiogenesis (**Figures 4** and **5**). Notably, all mice remained healthy throughout the experiment, exhibiting stable weights (**Additional Figure 8**). In general, fibrosis refers to the accumulation of extracellular matrix components in the dermis, resulting in modifications in its architecture. After the transplantation, an influx of immune cells occurs, initiating the early inflammatory phase and inducing tissue growth. Over time, chronic inflammation occurs, accompanied by fibrosis. Notably, macrophages play a vital role in fibrosis. We observed that the PCL/MeHA composite scaffold composed of MeHA with the highest molecular weight, i.e., the DS72-900 MeHA hydrogel, induced the most severe FBR, likely attributable to its significant stiffness. The MeHA hydrogel strongly influenced the stiffness of the PCL/MeHA composite scaffold, resulting in the PCL/DS72-900 MeHA composite scaffold exhibiting the highest stiffness. The stiffness of a biomaterial has been noted to influence macrophage-immune responses.[28] Increased stiffness can lead to changes in macrophage polarisation and migration patterns. Specifically, stiffer substrates can enhance the anti-inflammatory polarisation of macrophages.[29] The DS72-900 MeHA hydrogel with the highest stiffness triggered the more severe FBR, potentially because of more notable contact interaction with the macrophages and surrounding tissue. The level of angiogenesis was quantified by counting the number of blood vessels (**Figure 5**). However, vessel counting typically involves numerous challenges. First, the distribution of microvessel sizes and growth patterns vary within different

layers of the skin. Second, vWF, an endothelial cell marker, was used to identify and count vessels, necessitating the laborious selection of areas with high vessel density. Although we processed as many images as possible, artificial intelligence-based software could be used for more efficient and accurate quantification. Finally, the counting method involved several sources of bias because the blood vessels in the histological images exhibited different shapes and sizes owing to variations in the vessel orientation and sectioning direction. Thus, the determined number of blood vessels was used only for reference.

Although the mechanism of MeHA-induced angiogenesis remains largely unknown, it is likely to be similar to that of HA, as MeHA is a derivative of HA. HA can bind to cell HA receptor glycoproteins, such as cluster determinant molecule-44, receptors for hyaluronan-mediated motility, and Toll-like receptor-4,[30] promoting endothelial cell proliferation and migration and thereby inducing neoangiogenesis and sprout formation.[31] Moreover, HA with lower molecular weight has been noted to be more bioactive and thus capable of inducing stronger angiogenesis.[32, 33]

In conclusion, this study reported the fabrication and optimisation of PCL/MeHA composite scaffolds for subcutaneous transplantation. The scaffold composed of 3% PCL and DS70-100MeHA exhibited the least fibrosis and strong angiogenesis, potentially resulting in enhanced engraftment, survival, and retention in cell transplantation processes. Future studies can be aimed at using PCL/MeHA composite scaffolds for encapsulating and transplanting cells for therapeutic applications. In particular, such scaffolds can potentially isolate implanted cells from the host immune cells, improve cell survival, and aid the maintenance of cell functions.

Author contributions

HY, ZY and CX conceived and designed the analysis; HY, MZ, YZ and QZ collected and analyzed the data; CL, JHCL, KWYC and HW contributed analysis tools; HY, XZ, ZY, and CX wrote the paper. All authors approved the final version of the manuscript.

Financial support

This study was supported by Collaborative Research Fund from the Research Grants Council (RGC) of the Hong Kong Special Administrative Region China, No. C5044-21G, and Research Institute of Tsinghua at Pearl River Delta, No. 9239094 (both to CX).

Acknowledgement

All authors acknowledge the professional English language editing support provided by AsiaEdit (asiaedit.com).

Conflicts of interest statement

The authors declare no conflict of interest.

Open access statement

This is an open access journal, and articles are distributed under the terms of the Creative Commons Attribution-NonCommercial-ShareAlike 4.0 License, which allows others to remix, tweak, and build upon the work non-commercially, as long as appropriate credit is given and the new creations are licensed under the identical terms.

Additional files

Additional Figure 1: ^{1}H-Spectroscopy spectrum of MeHA (in D_2O).

Additional Figure 2: Storage modulus (G') and loss modulus (G'') of unmodified HA solutions (5% (w/w)).

Additional Figure 3: The swelling behaviors of crosslinked MeHA polymers in PBS.

Additional Figure 4: SEM images of the porous PCL scaffolds prepared by using different PCL/NaCl composition.

Additional Figure 5: Raw data from tensile elastic modulus tests of PCL scaffolds.

Additional Figure 6: Raw data from compressive elastic modulus tests of PCL scaffolds.

Additional Figure 7: Cell viability indicated the biocompatibility of PCL/MeHA composite scaffold.

Additional Figure 8: The *in vivo* experiment design and continuous mice body weight record.

Additional Figure 9: Comparison of angiogenesis situation of all scaffolds before and 4 weeks after transplantation.

1. Liu, D.; Bobrovskaya, L.; Zhou, X. F. Cell Therapy for neurological disorders: the perspective of promising cells. *Biology (Basel).* **2021**, *10*, 1142.
2. Hoang, D. M.; Pham, P. T.; Bach, T. Q.; Ngo, A. T. L.; Nguyen, Q. T.; Phan, T. T. K.; Nguyen, G. H.; Le, P. T. T.; Hoang, V. T.; Forsyth, N. R.; Heke, M.; Nguyen, L. T. Stem cell-based therapy for human diseases. *Signal Transduct Target Ther.* **2022**, *7*, 272.
3. De Pieri, A.; Rochev, Y.; Zeugolis, D. I. Scaffold-free cell-based tissue engineering therapies: advances, shortfalls and forecast. *NPJ Regen Med.* **2021**, *6*, 18.
4. Chan, B. P.; Leong, K. W. Scaffolding in tissue engineering: general approaches and tissue-specific considerations. *Eur Spine J.* **2008**, *17 Suppl 4*, 467-479.
5. Pina, S.; Ribeiro, V. P.; Marques, C. F.; Maia, F. R.; Silva, T. H.; Reis, R. L.; Oliveira, J. M. Scaffolding strategies for tissue engineering and regenerative medicine applications. *Materials (Basel).* **2019**, *12*, 1824.
6. Peña, J.; Corrales, T.; Izquierdo-Barba, I.; Doadrio, A. L.; Vallet-Regí, M. Long term degradation of poly(ε-caprolactone) films in biologically related fluids. *Polym Degrad Stab.* **2006**, *91*, 1424-1432.
7. Chang, C. Y.; Chan, A. T.; Armstrong, P. A.; Luo, H. C.; Higuchi, T.; Strehin, I. A.; Vakrou, S.; Lin, X.; Brown, S. N.; O'Rourke, B.; Abraham, T. P.; Wahl, R. L.; Steenbergen, C. J.; Elisseeff, J. H.; Abraham, M. R. Hyaluronic acid-human blood hydrogels for stem cell transplantation. *Biomaterials.* **2012**, *33*, 8026-8033.
8. Mahsa Khatami, S.; Parivar, K.; Naderi Sohi, A.; Soleimani, M.; Hanaee-Ahvaz, H. Acetylated hyaluronic acid effectively enhances chondrogenic differentiation of mesenchymal stem cells seeded on electrospun PCL scaffolds. *Tissue Cell.* **2020**, *65*, 101363.
9. Chang, H.; Zheng, M.; Yu, X.; Than, A.; Seeni, R. Z.; Kang, R.; Tian, J.; Khanh, D. P.; Liu, L.; Chen, P.; Xu, C. A swellable microneedle patch to rapidly extract skin interstitial fluid for timely metabolic analysis. *Adv Mater.* **2017**, *29*, 1702243.
10. Fryhofer, G. W.; Zlotnick, H. M.; Stoeckl, B. D.; Farrell, M. J.; Steinberg, D. R.; Mauck, R. L. Fabrication and maturation of integrated biphasic anatomic mesenchymal stromal cell-laden composite scaffolds for osteochondral repair and joint resurfacing. *J Orthop Res.* **2021**, *39*, 2323-2332.
11. Shin, J.; Lee, J. S.; Lee, C.; Park, H. J.; Yang, K.; Jin, Y.; Ryu, J. H.; Hong, K. S.; Moon, S. H.; Chung, H. M.; Yang, H. S.; Um, S. H.; Oh, J. W.; Kim, D. I.; Lee, H.; Cho, S. W. Tissue adhesive catechol-modified hyaluronic acid hydrogel for effective, minimally invasive cell therapy. *Adv Funct Mater.* **2015**, *25*, 3814-3824.
12. Trujillo-Lemon, M.; Bowman, C. N.; Stansbury, J. W. pH-responsive hydrogel with controlled swelling and degradation rate. 2005 NSTI Nanotechnology Conference and Trade Show - NSTI Nanotech 2005 Technical Proceedings. **2014**.
13. Smink, A. M.; Rodriquez, S.; Li, S.; Ceballos, B.; Corrales, N.; Alexander, M.; Koster, T.; de Haan, B. J.; Lakey, J. R. T.; de Vos, P.

Successful islet transplantation into a subcutaneous polycaprolactone scaffold in mice and pigs. *Transplantation direct.* **2023**, *9*, e1417.

14. Smink, A. M.; Li, S.; Hertsig, D. T.; de Haan, B. J.; Schwab, L.; van Apeldoorn, A. A.; de Koning, E.; Faas, M. M.; Lakey, J. R.; de Vos, P. The efficacy of a prevascularized, retrievable poly(D,L,-lactide-co-ε-caprolactone) subcutaneous scaffold as transplantation site for pancreatic islets. *Transplantation.* **2017**, *101*, e112-e119.
15. Intranuovo, F.; Gristina, R.; Brun, F.; Mohammadi, S.; Ceccone, G.; Sardella, E.; Rossi, F.; Tromba, G.; Favia, P. Plasma modification of PCL porous scaffolds fabricated by solvent-casting/particulate-leaching for tissue engineering. *Plasma Process Polym.* **2014**, *11*, 184-195.
16. Cho, Y. S.; Hong, M. W.; Kim, Y. Y.; Cho, Y. S. Assessment of cell proliferation in salt-leaching using powder (SLUP) scaffolds with penetrated macro-pores. *J Appl Polym Sci.* **2014**, *131*, 40240.
17. Mota, C.; Puppi, D.; Dinucci, D.; Gazzarri, M.; Chiellini, F. Additive manufacturing of star poly(ε-caprolactone) wet-spun scaffolds for bone tissue engineering applications. *J Bioact Compat Polym.* **2013**, *28*, 320-340.
18. Guarino, V.; Causa, F.; Ambrosio, L. Porosity and mechanical properties relationship in PCL porous scaffolds. *J Appl Biomater Biomech.* **2007**, *5*, 149-157.
19. Gupta, B.; Patra, S.; Ray, A. R. Preparation of porous polycaprolactone tubular matrix by salt leaching process. *J Appl Polym Sci.* **2012**, *126*, 1505-1510.
20. Kinney, S. M.; Ortaleza, K.; Vlahos, A. E.; Sefton, M. V. Degradable methacrylic acid-based synthetic hydrogel for subcutaneous islet transplantation. *Biomaterials.* **2022**, *281*, 121342.
21. Schindelin, J.; Arganda-Carreras, I.; Frise, E.; Kaynig, V.; Longair, M.; Pietzsch, T.; Preibisch, S.; Rueden, C.; Saalfeld, S.; Schmid, B.; Tinevez, J. Y.; White, D. J.; Hartenstein, V.; Eliceiri, K.; Tomancak, P.; Cardona, A. Fiji: an open-source platform for biological-image analysis. *Nat Methods.* **2012**, *9*, 676-682.
22. Schneider, C. A.; Rasband, W. S.; Eliceiri, K. W. NIH image to ImageJ: 25 years of image analysis. *Nat Methods.* **2012**, *9*, 671-675.
23. Kim, M. H.; Nguyen, H.; Chang, C. Y.; Lin, C. C. Dual functionalization of gelatin for orthogonal and dynamic hydrogel cross-linking. *ACS Biomater Sci Eng.* **2021**, *7*, 4196-4208.
24. Zhang, D.; Chen, Q.; Shi, C.; Chen, M.; Ma, K.; Wan, J.; Liu, R. Dealing with the foreign-body response to implanted biomaterials: strategies and applications of new materials. *Adv Funct Mater.* **2021**, *31*, 2007226.
25. Anderson, J. M.; Rodriguez, A.; Chang, D. T. Foreign body reaction to biomaterials. *Semin Immunol.* **2008**, *20*, 86-100.
26. Janmohammadi, M.; Nourbakhsh, M. S.; Bahraminasab, M.; Tayebi, L. Effect of pore characteristics and alkali treatment on the physicochemical and biological properties of a 3D-printed polycaprolactone bone scaffold. *ACS Omega.* **2023**, *8*, 7378-7394.
27. Kim, J. W.; Shin, K. H.; Koh, Y. H.; Hah, M. J.; Moon, J.; Kim, H. E. Production of poly(ε-caprolactone)/hydroxyapatite composite scaffolds with a tailored macro/micro-porous structure, high mechanical properties, and excellent bioactivity. *Materials (Basel).* **2017**, *10*, 1123.
28. Ni, Y.; Qi, H.; Zhang, F.; Jiang, S.; Tang, Q.; Cai, W.; Mo, W.; Miron, R. J.; Zhang, Y. Macrophages modulate stiffness-related foreign body responses through plasma membrane deformation. *Proc Natl Acad Sci U S A.* **2023**, *120*, e2213837120.
29. Sridharan, R.; Cavanagh, B.; Cameron, A. R.; Kelly, D. J.; O'Brien, F. J. Material stiffness influences the polarization state, function and migration mode of macrophages. *Acta Biomater.* **2019**, *89*, 47-59.
30. Zhang, C.; Yuan, Y.; Wu, K.; Wang, Y.; Zhu, S.; Shi, J.; Wang, L.; Li, Q.; Zuo, X.; Fan, C.; Chang, C.; Li, J. Driving DNA origami assembly with a terahertz wave. *Nano Lett.* **2022**, *22*, 468-475.
31. Zhang, C.; Jing, X.; Guo, L.; Cui, C.; Hou, X.; Zuo, T.; Liu, J.; Shi, J.; Liu, X.; Zuo, X.; Li, J.; Chang, C.; Fan, C.; Wang, L. Remote photothermal control of DNA origami assembly in cellular environments. *Nano Lett.* **2021**, *21*, 5834-5841.
32. Pardue, E. L.; Ibrahim, S.; Ramamurthi, A. Role of hyaluronan in angiogenesis and its utility to angiogenic tissue engineering. *Organogenesis.* **2008**, *4*, 203-214.
33. Zhang, C.; Xia, D.; Liu, J.; Huo, D.; Jiang, X.; Hu, Y. Bypassing the immunosuppression of myeloid-derived suppressor cells by reversing tumor hypoxia using a platelet-inspired platform. *Adv Funct Mater.* **2020**, *30*, 2000189.

Received: December 11, 2023
Revised: January 20, 2024
Accepted: March 8, 2024
Available online: March 28, 2024